World Academy of Science, Engineering and Technology
International Journal of Mechanical and Mechatronics Engineering
Vol:5, No:1, 2011

Effect of Helium-Argon Mixtures on the Heat Transfer and Fluid Flow in Gas Tungsten Arc Welding

A. Traidia[*,1, 2], F. Roger[1], A. Chidley[1], J. Schroeder[2], T. Marlaud[2]

***Abstract*—**A transient finite element model has been developed to study the heat transfer and fluid flow during spot Gas Tungsten Arc Welding (GTAW) on stainless steel. Temperature field, fluid velocity and electromagnetic fields are computed inside the cathode, arc-plasma and anode using a unified MHD formulation. The developed model is then used to study the influence of different helium-argon gas mixtures on both the energy transferred to the workpiece and the time evolution of the weld pool dimensions. It is found that the addition of helium to argon increases the heat flux density on the weld axis by a factor that can reach 6.5. This induces an increase in the weld pool depth by a factor of 3. It is also found that the addition of only 10% of argon to helium decreases considerably the weld pool depth, which is due to the electrical conductivity of the mixture that increases significantly when argon is added to helium.

***Keywords*—**GTAW, Thermal plasmas, Fluid flow, Marangoni effect, Shielding Gases.

I. Introduction

GAS Tungsten Arc Welding (GTAW), also known as Tungsten Inert Gas Welding (TIG) is widely used for the manufacturing of ships, pipelines, automotive and many heavy nuclear components. The numerical simulation of such a process has become a big challenge because it permits to get a good prediction of the welded joint characteristics as function of the welding input parameters. Then it improves the welding quality and increases productivity. To ensure the current flow, and protect the weld, a shielding gas flows through a nozzle surrounding the cathode. As seen in Fig. 1, the complexity of the numerical simulation is due to the strong coupling between many physics involved in this process. The ionization of the shielding gas ensures the current flow between the two electrodes, then the heating Joule effect creates a thermal plasma composed of electrons, ions and neutral species at a large temperature range; from 300 K to more than 20 000 K. The workpiece is then heated from both the arc-plasma conduction, and the electrons flow at the top surface. Depending on the melting temperature of the workpiece, a weld pool is formed in which the fluid flow is governed by the Marangoni effect at the top surface, the buoyancy forces and the electromagnetic forces created by the current flow.

Due to its low cost, argon is the most common used shielding gas, but with the disadvantage of a low heat transferred to the workpiece. The weld pool dimensions (depth and width) are then limited compared to welding under other shielding gases.

In the manufacturing industry, argon is sometimes mixed to helium to increase the weld pool depth, but the content of each gas in the mixture is usually determined by experimental tests.

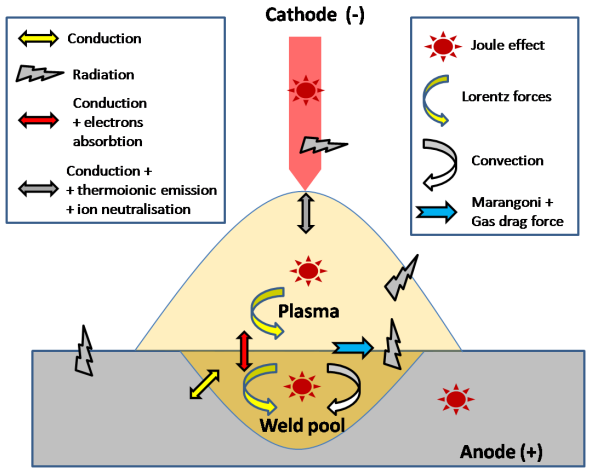

Fig. 1. Main coupled phenomena in arc welding simulation

Many numerical models of spot GTAW are available in the literature [1-5]. Most of them consider only one part of the welding process [1-4] (either the cathode, or the arc plasma, or the anode) which leads to assume some boundary conditions that do not represent the real situations. The best way to deal with the problem is to take into account the three parts (anode, cathode and arc-plasma) in a unified formalism. The interfaces between the plasma and the electrodes are then considered as internal boundaries. This approach was proposed by Lowke and Tanaka *et al* [5] and gives satisfying results for constant current welding. Recently, Murphy *et al* [6] used this approach to investigate the effectiveness of different shielding gas

* Corresponding author:
Full name: Abderrazak Traidia
Academic title/degree: PhD Mechanical Engineering
Working place: France
Research field: Multiphysics couplings, Welding simulations
Email: abderrazak.traidia@ensta-paristech.fr
Post address: [1, 2]
[1] Laboratory of Mechanics, Materials and Structures Group ENSTA-ParisTech, Chemin de la Hunière, 91120 Palaiseau Cedex, France.

[2] The Technical Center AREVA NP, BP 40001 Saint Marcel, 71328 Chalon Sur Saone Cedex, France.

mixtures for arc welding. However, calculations were performed for a water-cooled anode, without weld pool. Murphy *et al* [7] performed calculations for argon and helium with a molten stainless steel anode taking into account the metal vapors, but with some limitations: (1) a constant surface tension coefficient was assumed which has a great influence on the predicted molten zone; (2) argon-helium mixtures were not considered.

In the present work, a unified finite element model is introduced taking into account the three parts of the welding process (cathode, arc-plasma, and anode). The surface tension coefficient which mainly governs the fluid flow inside the weld pool is taken as dependent on both the sulfur content of the steel and temperature. Different argon-helium mixtures can be considered as a shielding gas. The influence of the helium mole fraction in the mixture on the heat flux, current density and weld pool evolution are computed. Comsol Script© software is used to implement our numerical model.

II. Mathematical formulation

A. Governing equations

The following assumptions are considered for the mathematical formulation of the multiphysics problem:

- The study is restricted to spot GTAW; an axisymmetric coordinate system is used.
- The arc column is assumed to be at Local Thermodynamic Equilibrium (LTE) and the influence of metal vapors on the plasma properties is not considered.
- The gas plasma and molten metal are incompressible.

The velocity and pressure field are calculated in the plasma and anode domains, and the temperature field is computed in the three regions using the classical conservation equations, as follows:

(1) *Conservation of mass*

$$\nabla \cdot \vec{v} = 0 \tag{1}$$

(2) *Conservation of momentum*

$$\rho\left(\frac{\partial \vec{v}}{\partial t} + \vec{v}\cdot\nabla\vec{v}\right) = -\nabla p + \nabla\cdot\left[\mu\left(\nabla\vec{v} + {}^{t}\nabla\vec{v}\right)\right] + \vec{j}\times\vec{B} + \rho_0\vec{g}\left(1 - w_p\beta\left(T - T_{ref}\right)\right) \tag{2}$$

(3) *Conservation of energy*

$$\rho c_p^{eq}\left(\frac{\partial T}{\partial t} + \vec{v}\cdot\nabla T\right) = \nabla\cdot\left(k\nabla T\right) + S_v \tag{3}$$

Where $\vec{v}$ is velocity, T is temperature, p is pressure, ρ_0 equals the gas density in the plasma domain and a reference density in the anode region, $c_p^{eq} = c_p + w_p L_f (df_L / dT)$ is an equivalent specific heat that takes into account the latent heat of fusion L_f. f_L is the liquid fraction assumed to vary linearly with temperature in the mushy zone and w_p equals 1 in the weld pool and 0 elsewhere. β is the metal thermal expansion and T_{ref} is taken as the solidus temperature.

In the anode and cathode regions, the volumetric heat source is the Joule effect

$$S_v = \vec{j}\cdot\vec{E}$$

Whereas in the arc plasma region the enthalpic flux and radiation losses are added

$$S_v = \vec{j}\cdot\vec{E} + \frac{5k_B}{2e}\vec{j}\cdot\nabla T - 4\pi\varepsilon_N$$

The determination of the electromagnetic forces and the joule effect in both arc plasma and workpiece requires the computation of the current density $\vec{j}$ and the magnetic flux $\vec{B}$. To achieve this, the coupled current continuity and the magnetic potential equations are computed as function of the electric potential V and the magnetic potential vector $\vec{A}$ as follows:

$$\nabla\cdot\left(\sigma\nabla V\right) = 0 \tag{4}$$

$$\nabla\times\left(\frac{1}{\mu_0}\nabla\times\vec{A}\right) + \sigma\nabla V = \vec{0} \tag{5}$$

The current density, electric field and magnetic flux are then computed from V and $\vec{A}$ as follows:

$$\vec{E} = -\nabla V;\quad \vec{j} = -\sigma\nabla V;\quad \vec{B} = \nabla\times\vec{A} \tag{6}$$

B. Boundary conditions

The computational domain is shown in Fig. 2. All the boundary conditions are listed in Table I; the most important points are discussed below;

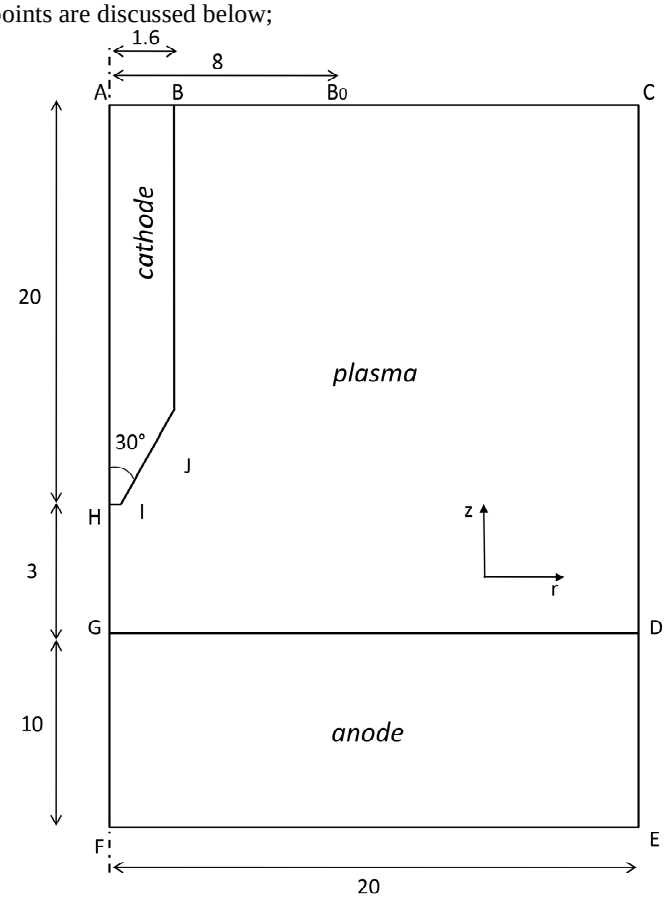

Fig. 2. Computational domain (dimensions in mm)

- At the interface between arc plasma and the anode (GD) the following conditions must be satisfied:

$$\left[-k\nabla T\cdot(-\vec{n})\right]_{anode}=\left[-k\nabla T\cdot(-\vec{n})\right]_{plasma}+\left|\vec{j}\cdot\vec{n}\right|\phi_a-\varepsilon\sigma_B T^4 \quad (7)$$

$$\mu\frac{\partial(\vec{v}\cdot\vec{s})}{\partial\vec{n}}=\vec{\tau}_a+f_L\frac{\partial\gamma}{\partial T}\frac{\partial T}{\partial\vec{s}} \quad (8)$$

The first condition means that the normal heat flux at the anode is composed by the heating conduction flux from the plasma, the electrons condensation flux $\left|\vec{j}\cdot\vec{n}\right|\phi_a$ (which represents the energy transferred from the electrons to the anode) and the cooling radiation losses $\varepsilon\sigma_B T^4$. ϕ_a is the anode work function and σ_B is the Stefan-Boltzmann constant.

The second condition means that the total shear stress at the top surface of the weld pool is the sum of the arc drag force $\vec{\tau}_a$, and the Marangoni force. $\vec{s}$ and $\vec{n}$ are respectively a local tangent vector and the normal vector to the top free surface ($\vec{n}$ is directed toward the plasma domain). $\partial\gamma/\partial T$ is the surface tension coefficient, which has been reported to have a big impact on the flow directions inside the weld pool [1-4]. This coefficient is negative for pure metals, but can be altered from a negative to a positive value by the presence of surface-active elements, such as sulfur and oxygen.

When the soluble sulfur or oxygen concentration is below a certain critical concentration, the surface tension is highest at the edges of the pool, and the thermocapillary flow is outward from low to high surface tension and results in a wide and shallow weld. However, when oxygen or sulfur concentration is above the critical content, surface flow is inward, and hot liquid is swept to the bottom of the pool and produces a narrow and deep weld. In the case of stainless steel, the main surface active element is sulfur, the dependence of $\partial\gamma/\partial T$ on temperature T and sulfur activity a_s is considered using the expression developed by Sahoo *et al.* [8] as follows:

$$\frac{\partial\gamma}{\partial T}=-A_\gamma-R_g\Gamma_s\ln(1+Ka_s)-\frac{Ka_s}{1+Ka_s}\Gamma_s\frac{\Delta H_0}{T} \quad (9)$$

$$K(T)=k_1\exp\left(-\frac{\Delta H_0}{R_g T}\right)$$

The main constants appearing in the above expression are detailed later in this paper.

- Along the interface between the arc plasma and the cathode (HIJB), the following condition must be considered:

$$\left[-k\nabla T\cdot(-\vec{n})\right]_{cathode}=\left[-k\nabla T\cdot(-\vec{n})\right]_{plasma}+j_i V_i-j_e\phi_c-\varepsilon\sigma_B T^4 \quad (10)$$

Where V_i and ϕ_c are respectively the argon ionization potential and the cathode work function. j_i and j_e are respectively the ion current and electron current. The above condition means that the heat flux transferred to the cathode is the sum of the conduction flux from the arc-plasma, the ion heating (energy received by the cathode from the collected ions), the cooling thermionic emission (energy absorbed by the emitted electrons from the cathode), and the radiation cooling losses. The ion and electron currents are calculated using the following expressions [5]:

$$j_e=\begin{cases} j_r & \text{if } \left(\left|\vec{j}\cdot\vec{n}\right|-j_r\right)>0 \\ \left|\vec{j}\cdot\vec{n}\right| & \text{if } \left(\left|\vec{j}\cdot\vec{n}\right|-j_r\right)\le 0 \end{cases};\quad j_i=\left|\vec{j}\cdot\vec{n}\right|-j_e \quad (11)$$

$$j_r=A_r T^2\exp\left(-e\phi_e/k_B T\right)$$

Where, A_r, ϕ_e and e are respectively the Richardson's constant, the effective work function for thermionic emission and the elementary charge.

- Along the bottom surface of the anode, heat losses are considered using the following relation [11]:

$$\vec{q}\cdot\vec{n}=h_c(T-T_0)\quad\text{with}\quad h_c=24.1\times10^{-4}\times0.9\times T^{1.61} \quad (12)$$

TABLE I
BOUNDARY CONDITIONS

AB	$T=T_0;\quad \vec{j}\cdot\vec{n}=\dfrac{I}{\pi R_c^{\,2}}$
BB0	$T=T_0;\quad \vec{v}\cdot\vec{n}=-Ugaz;\quad \vec{j}\cdot\vec{n}=0;\quad \vec{A}\times\vec{n}=0$
B0C CD	$T=T_0;\quad \vec{j}\cdot\vec{n}=0;\quad p=p_0;$ $\vec{n}\cdot\underline{\underline{\tau}}\cdot\vec{n}=0;\quad \vec{A}\times\vec{n}=\vec{0}$
DE EF	$\vec{q}\cdot\vec{n}=h_c(T-T_0);\quad \vec{v}=\vec{0};\quad V=0;\quad \vec{A}\times\vec{n}=0$
FA	$\vec{q}\cdot\vec{n}=0;\quad \vec{v}\cdot\vec{n}=0;\quad \vec{j}\cdot\vec{n}=0;\quad \vec{B}=\vec{0}$
GD	$\left[-k\nabla T\cdot(-\vec{n})\right]_{anode}=\left[-k\nabla T\cdot(-\vec{n})\right]_{plasma}+\left\|\vec{j}\cdot\vec{n}\right\|\phi_a-\varepsilon\sigma_B T^4$ $\mu\dfrac{\partial(\vec{v}\cdot\vec{s})}{\partial\vec{n}}=\vec{\tau}_a+f_L\dfrac{\partial\gamma}{\partial T}\dfrac{\partial T}{\partial\vec{s}}$ $\vec{v}\cdot\vec{n}=0;\quad \left[\!\left[\vec{j}\cdot\vec{n}\right]\!\right]=0$
HB	$\left[-k\nabla T\cdot(-\vec{n})\right]_{cathode}=\left[-k\nabla T\cdot(-\vec{n})\right]_{plasma}+j_i V_i-j_e\phi_c-\varepsilon\sigma_B T^4$ $\vec{v}=\vec{0};\quad \left[\!\left[\vec{j}\cdot\vec{n}\right]\!\right]=0$

C. Modeling of the arc-electrodes interfaces

Physically, between the plasma column and the two electrodes a thin layer exits which is not in LTE. In fact, the heavy particles temperature is close to the electrodes materials temperature (2000 K-3500 K), whereas the electron temperature is much higher in order to ensure the current conduction between the plasma and the electrodes. To avoid the development of a twin temperature model (electrons temperature and ions temperature) which is very consuming in term of computing time, we assume the anodic and cathodic zones to be an ohmic conductor, which ensures the transition between the plasma column and the electrodes. In order to achieve this, we add two thin layers respectively adjacent to the anode and to the cathode; within these layers we will consider the electric conductivity of the corresponding electrode and the viscosity, thermal conductivity and specific heat of the plasma gas. The thickness of these layers is about 1.10^{-4} m which is the length of the non-LTE zone near the electrodes. This method was suggested by Lago and Gonzalez *et al* [9, 10] and was applied only for the anodic zone and it is extended in this paper for the cathodic zone.

D. Thermophysical properties

The workpiece is a 304L ss disk containing 40 ppm of sulfur. Its thermophysical properties are given in Table II.

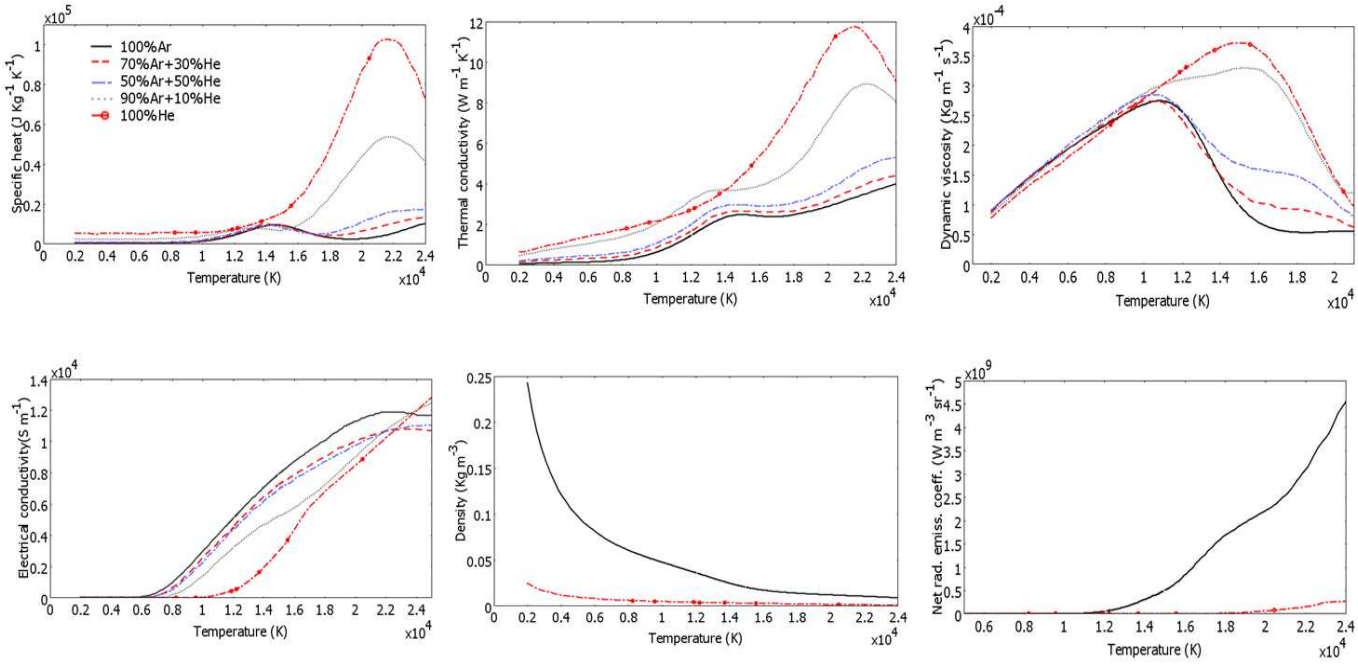

Fig. 3. Thermophysical and transport properties of argon-helium mixtures as function of temperature, taken from [10]

The thermodynamic and transport properties of helium-argon plasmas are taken from the previous works of Murphy *et al* [12], and are shown in Fig. 3.

The net radiative emission coefficient and the density of each argon-helium mixture are determined using a mole-fraction-weighted sum of the coefficients and densities of the component gases as follows:

$$\varepsilon_{N_{mixture}} = x_{Ar}\varepsilon_{N_{Ar}} + x_{He}\varepsilon_{N_{He}}$$
$$\rho_{mixture} = x_{Ar}\rho_{Ar} + x_{He}\rho_{He} \quad (13)$$

Where x_{Ar}, and x_{He} are respectively the mole fraction of argon and helium in the mixture.

TABLE II
MATERIALS PROPERTIES OF 304L STAINLESS STEEL

Symbol	Quantity	Value
ρ	Density	6080 to 7272 kg.m^{-3}
c_p	Specific heat	510 to 796 J.kg^{-1}.K^{-1}
k	Thermal conductivity	15.2 to 42.8 W.m^{-1}.K^{-1}
μ	Dynamic viscosity	0.03 kg.m^{-1}.s^{-1}
σ	Electrical conductivity	7.7 ×10^5 Ω^{-1}.m^{-1}
ε	Anode emissivity	0.9
T_l	Liquidus temperature	1723 K
T_s	Solidus temperature	1673 K
a_s	Sulfur activity	0.004 wt%
R_g	Gas constant	8314 J.kg^{-1}.mole^{-1}.K^{-1}
ΔH_0	Latent heat of fusion	-1.88 × 10^8 J.kg^{-1}.mole^{-1}
Γ_s	Surface excess of sulfur at saturation	1.3 × 10^{-8} kg.mole.m^{-2}
γ_m	Surface tension at pure metal	1.943 N.m^{-1}
k_1	Entropy factor	3.18 × 10^{-3}
A_γ	Constant in surface tension gradient	4.3 × 10^{-4} N.m^{-1}.K^{-1}

III. NUMERICAL RESULTS AND DISCUSSION

The calculations are done for an arc current of 180 A, a cathode tip angle of 60°, an arc length of 3 mm and a total heating time of 8 s. We simulate the cases of pure argon, pure helium, and three different helium-argon mixtures to study the influence of helium mole fraction in the mixture. The gas inflow rate is fixed to 30 L/min for all cases.

The characteristics of TIG arc are highly dependent on the shielding gas composition. This is well shown in Fig. 4, which shows the temperature field and temperature contours in the arc plasma zone (the gap between two contours is 1000 K), as well as the normalized fluid velocity and streamlines inside the molten weld pool at the end of heating (t=8 s). The arc is bell shaped for argon which is in good agreement with the common experimental observations. As helium fraction in the mixture increases, the arc does not have the typical bell shape of argon but becomes more and more constricted. The addition of helium to argon increases the maximum temperature, which is due the high thermal conductivity of helium (see Fig. 3). The maximum plasma velocity also increases with helium mole fraction in the mixture; it almost increases by a factor of 4 from pure argon arc to pure helium arc. This is mainly due to the magnetic pinch effect that is more important for helium arc (because of the arc constriction).

Fig. 4 shows also that there are two vortices near the top surface of the weld pool; an inward flow near the edges of the weld pool, and an outward flow near the center of the weld pool. The formation of these vortices is explained by the sign of the surface tension coefficient $\partial\gamma/\partial T$; above a critical temperature (that depends on the sulfur activity of the alloy),

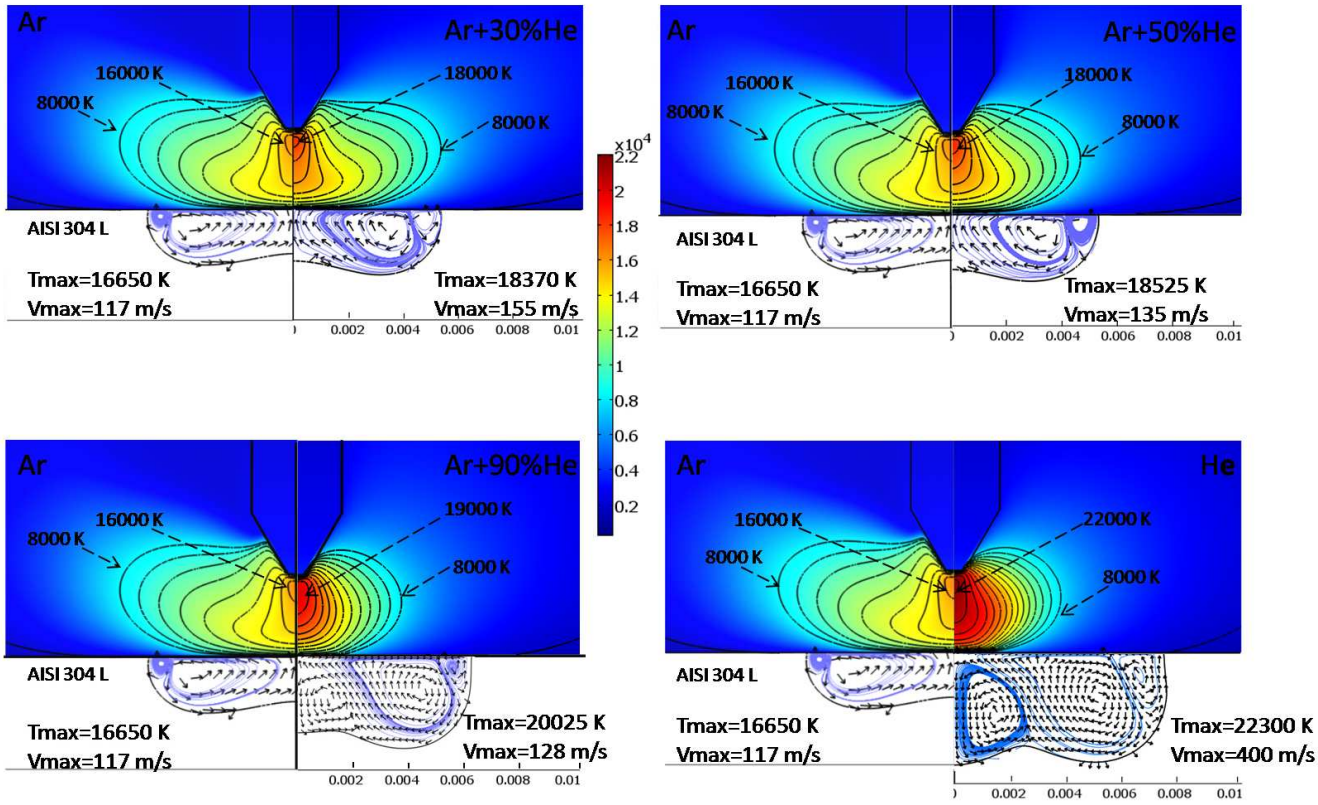

Fig. 4. Plasma temperature field, temperature contours, normalized molten metal velocity and streamlines inside the weld pool at the final time of welding t=8s.

$\partial\gamma/\partial T$ becomes negative leading to the formation of two vortices corresponding to the regions where the surface tension coefficient is negative or positive. Details about the formation of these vortices and their evolution with time can be found in our previous works [4]. It is well seen that the addition of helium leads to the formation of a new vortex that creates an inward flow and thus increases the weld pool depth. This goes with the experimental tests which show that the weld pool depth increases with the addition of helium into the shielding gas. The appearing of the new vortex is mainly explained by the increasing level of electromagnetic forces inside the weld pool due to the addition of helium.

The radial evolution of the heat flux and current density at the anode for the different gas mixtures are respectively shown in Fig. 5 and Fig. 6. The addition of any fraction of helium to argon leads to increase the heat flux and current density at the top surface of the weld pool. It is remarkable to see that the addition of up to 90% of helium to argon leads to increase the heat flux density on the axis by a factor of 2.3, whereas the 100% helium arc increases the heat flux density on the axis by a factor of 6.5. This is explained by the lower electrical conductivity of pure He than that of pure Ar or He-Ar mixtures (see Fig. 3).

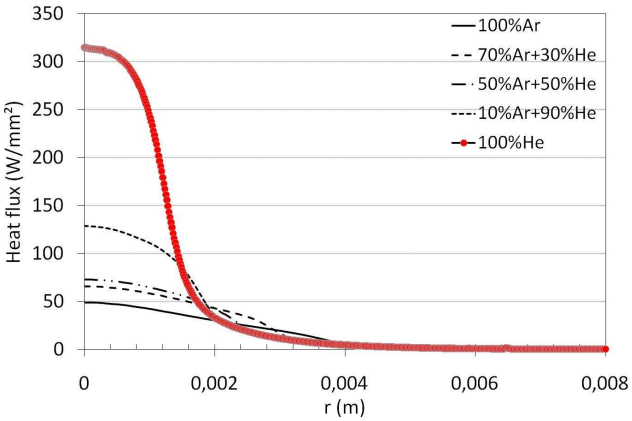

Fig. 5. Radial evolution of the heat flux density at the anode

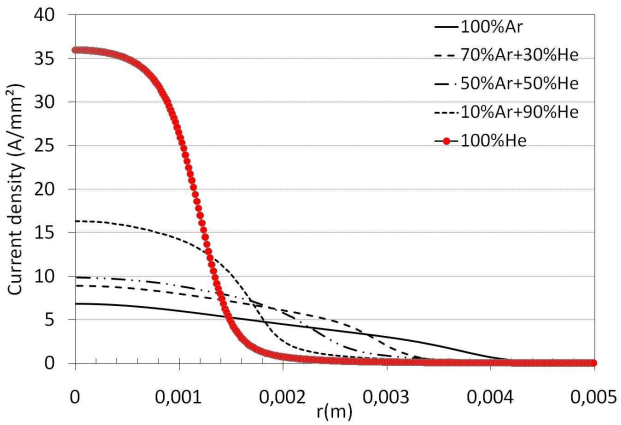

Fig. 6. Radial evolution of the current density at the anode

Even for a (10% He, 90% Ar) mixture, the electrical conductivity is closer to pure argon than to pure helium. This leads to reduce the diameter of the current channel and leads to the constriction of the zone through which heat and current flow.

Now, turn to the effect of helium fraction in the mixtures on the weld pool dimensions. The time evolution of the weld pool half-width and depth for the different studied gas mixtures are shown in Fig. 7 and Fig. 8. As seen, adding helium to argon has a great impact on the weld pool dimensions. In particular, it has a significant importance on the weld pool depth. The final depth of the weld pool triples between pure argon arc and pure helium arc. This is due to the inward vortex created during helium arc that leads to increase the weld pool depth. By comparing the 90% He case with the pure helium case, we can notice that the addition of only 10% of argon decreases the weld pool depth by around 40%. This is the consequence of the decrease in the heat flux intensity when adding argon to helium (discussed previously and shown in Fig. 5).

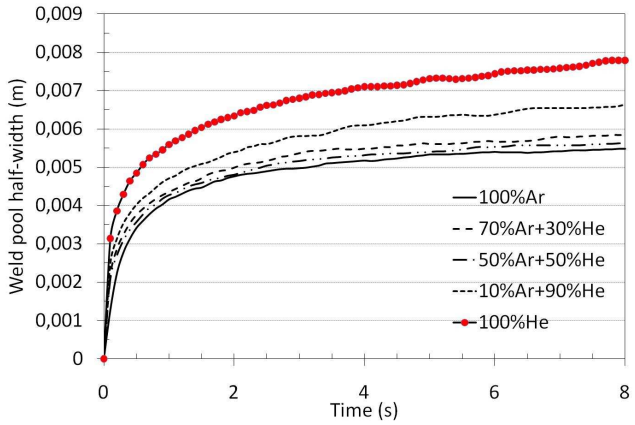

Fig. 7. Weld pool half-width as function of time for different gas mixtures

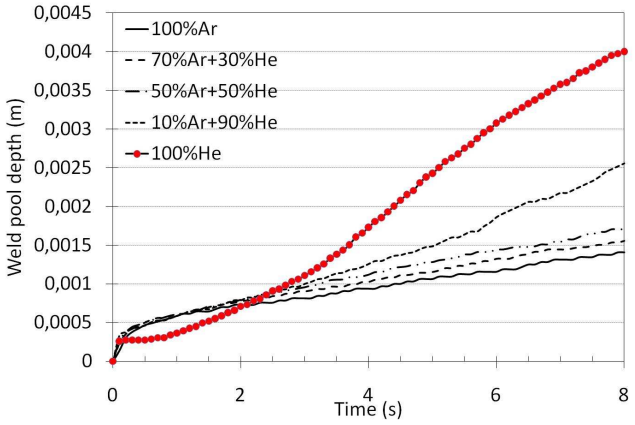

Fig. 8. Weld pool depth as function of time for different gas mixtures

IV. Conclusion

A numerical investigation of the effectiveness of different helium-argon mixtures on the heat transfer and fluid flow during GTAW was presented in this paper. The addition of helium to argon was found to have significant impacts on the arc properties; (1) it increases both the plasma temperature and gas velocity on the axis, (2) the arc is more constricted due to the lower electrical conductivity of helium, (3) it increases the heat flux and current density at the anode as well as the total energy transferred to the workpiece, and (4) the change in the energy transfer due to the addition of helium has an important influence on the fluid flow inside the molten weld pool, then the weld pool dimensions are affected; in particular, the weld depth is increased by a factor of 3 between pure argon and pure helium arc.

Acknowledgment

This research was supported by the Technical Center of AREVA NP, FRANCE. The authors are grateful to Alexander Chidley and Lahcene Cherfa for their great support.

References

[1] W.H. Kim, and S.J. Na, "Heat and fluid flow in pulsed current GTA weld pool", in *Int. J. Heat Mass Tran*., 1998, vol 41, pp. 3213-3227.
[2] H.G. Fan, H.L. Tsai, and S.J. Na, "Heat transfer and fluid flow in a partially or fully", in *Int. J. Heat Mass Tran*., 2001, vol 44, pp. 417-428.
[3] F. Lu, S. Yao, S. Lou, and Y. Li, "Modeling and finite element analysis on GTAW arc and weld pool", in *Comput. Mater. Sci.*, 2004, vol 29, pp. 371-378.
[4] A. Traidia, F. Roger, and E. Guyot, "Optimal parameters for pulsed gas tungsten arc welding in partially", in *Int. J. Therm. Sci*., 2010, vol 49, pp. 1197-1208.
[5] M. Tanaka, and J.J. Lowke, "Predictions of weld pool profiles using plasma physics", in *J. Phys. D: Appl. Phys*., 2007, vol 40, pp. R1-R23.
[6] A.B. Murphy, M. Tanaka, S. Tashiro, T. Sato, and J.J. Lowke, "A computational investigation of the effectiveness of different shielding gas mixtures for arc", in *J. Phys. D: Appl. Phys*., 2009, vol 42, 115205.
[7] A.B. Murphy *et al*, "Modeling of thermal plasmas for arc welding_ the role of the shielding gas properties and of metal vapour ", in *J. Phys. D: Appl. Phys*., 2009, vol 42, 194006.
[8] P. Sahoo, T. DebRoy, M.T. McNallan, "Surface tension of binary metal surface active solute systems under conditions relevant to welding metallurgy", in *Metall. Trans. B.*, 1988, vol 19B**,** pp. 483-491.
[9] F. Lago, JJ. Gonzalez, P. Freton, and A. Gleizes. "A numerical modelling of an electric arc and its interaction with the anode: Part I. The two-dimensional model", 2004, in *J. Phys. D: Appl. Phys*. Vol 37, pp. 883-897.
[10] JJ. Gonzalez, F. Lago, P. Freton, M. Masquère, and X. Franceries. "A numerical modelling of an electric arc and its interaction with the anode: Part II. The three-dimensional model- influence of external forces on the arc column", 2005, in *J. Phys. D: Appl. Phys*, vol 38, pp. 306-318.
[11] J. Goldak, M. Bibby, J. Moore, and B. Patel, "Computer modeling of heat flow in welds", in *Metall. Trans B.* 1986, vol 17, pp. 587-600.
[12] A.B. Murphy, "Transport coefficients of Helium and Argon-Helium plasmas", in *IEEE Transactions on plasma science*, 1997, vol. 25, n° 5.